JOURNAL OF MATERIALS SCIENCE, 30 (1995) 5178–5184

R-curve behaviour and microstructure of sintered silicon nitride

YOUNG-WOOK KIM*, M. MITOMO
National Institute for Research in Inorganic Materials, Ibaraki 305, Japan
N. HIROSAKI
Materials Research Laboratory, Nissan Research Centre, Nissan Motor Company Ltd, Yokosuka 237, Japan

R-curves for two *in situ* reinforced silicon nitrides A and B, of different microstructures, were characterized using indentation–crack growth measurements. Silicon nitride B, with its coarser microstructure and 8 MPa $m^{1/2}$ toughness, showed higher resistance to crack growth and more damage tolerance than silicon nitride A, with its finer microstructure and 7 MPa $m^{1/2}$ toughness. However, silicon nitride A showed a higher Weibull modulus than that of silicon nitride B due to the relatively narrow critical grain-size distribution. These results suggest that a coarse microstructure with narrow flaw-size distribution is beneficial to toughening, damage tolerance, and reliability.

1. Introduction

It is necessary to improve the reliability of sintered silicon nitride ceramics in order to widen their application as engineering materials. It has been shown that *in situ* reinforced silicon nitride ceramics exhibit increasing resistance to fracture with crack extension [1–3]. This behaviour is frequently referred to as "*R*-curve" behaviour, and they are referred as *R*-curve materials.

R-curve behaviour arises because additional energy is required in addition to that needed at the crack tip, to propagate the crack. The additional energy is possibly required to overcome the restraining forces of ligaments in the wake of the crack. Tortuous crack paths, such as crack bridging [4] and crack deflection [5], possibly constitute a systematic increase of the fracture resistance. Hence, *R*-curve materials have high fracture toughness and increased crack stabilization, which leads to diminished distribution of strengths for a given range of flaw sizes. It has been shown that the shape of the *R*-curve dictates the strength variability and the damage tolerance of the material [6–8], and the fracture toughness of silicon nitride is highly dependent on its microstructure [9, 10]. Therefore, an understanding of the relation between *R*-curve behaviour and microstructure of silicon nitride may be an effective means of achieving narrow strength distributions, i.e. reliable materials, independent of randomly introduced flaws.

In the present study, the *R*-curve behaviour for two *in situ* reinforced silicon nitrides A and B of different microstructures was investigated using the indentation–crack growth method. The indentation–crack growth method is believed to give a more reliable value than the indentation–strength method because it does not assume the crack-length dependence of fracture toughness, as is done in the indentation –strength method [1]. Although strength measurements of indented specimens were carried out to examine flaw-tolerance behaviour, *R*-curve behaviour by the indentation–strength method was not included in the present work because the method gave higher fracture resistances than acceptable values [1, 11]. Silicon nitride A was a commercial, pressureless sintered, *in situ* toughened silicon nitride with relatively fine microstructure, and silicon nitride B was a gas-pressure sintered, *in situ* toughened silicon nitride, fabricated from β-Si_3N_4 powder with relatively coarse microstructure. Microstructure analysis, indentation load–strength analysis (strength measured as a function of indentation load), and crack-wake observations were used to correlate the *R*-curve with the microstructure.

2. Experimental procedure

The silicon nitride A used in this study was a commercial, pressureless sintered, *in situ* toughened silicon nitride (Referceram SN, Japan Fine Ceramics Centre, Nagoya, Japan). Additives in the sintered materials were 3.38 wt % MgO, 4.15 wt % Ce_2O_3 and 0.84 wt % SrO (by atomic absorption spectroscopy). The silicon nitride B was fabricated as follows. The raw β-Si_3N_4 powder (Grade SN-P21FC, Denkikagaku, Tokyo,

* *Permanent address*: Korea Institute of Science and Technology, Seoul, Korea.

0022–2461

Japan), which was made by nitridation of silicon, and 4 mol % of an equimolar ratio of Al_2O_3 (A16-SG, Alcoa Industrial Chemicals, Bauxite, AR, USA) and Y_2O_3 (99.9% pure, Shin-etsu Chemical, Tokyo, Japan) were ball milled in ethanol for 24 h, dried, die pressed at 20 MPa and isostatically pressed at 200 MPa. The green compacts were fired at 2000 °C for 8 h under 1 MPa nitrogen.

Image analysis of the large elongated grains was conducted to evaluate the microstructural features quantitatively. Polished and plasma-etched specimens were examined by scanning electron microscopy (SEM) at magnifications of X1000 and X2000. The length, diameter, and area of each grain were measured using a Luzex III (Nireco Corporation, Tokyo, Japan). Grain diameter was defined as the minimum grain projection.

Specimens for the R-curve test were cut and polished to rectangular bars of dimensions of 3mm × 4mm × 40 mm with a 140 grit diamond wheel. The tensile surface was polished with 1 μm diamond paste to remove a residual stress due to machining and to produce a finish for optical microscopic examination. Prior to indentation, a thin film of moisture-free silicone oil was spread over the site of the indentation for minimizing moisture-assisted subcritical crack growth of as-indented cracks. Special care was taken to orient the radial cracks generated from the indentation parallel to the sides of the bar.

For establishing indentation load (P) –strength (S) relationship, three Vickers indentations with loads ranging from 2.94–490 N were made, 3 mm apart, in the centre of prospective tensile surface of each test piece. A total of approximately 30 indented bars for each of A and B were directly fractured using four-point bending to estabilish the indentation load–strength relationship. For four-point bending, 10 mm inner and 30 mm outer spans were used.

For crack-growth experiments, a Vickers indentation with loads ranging from 4.9–490 N was made at the centre of the prospective tensile surface of each test piece. A total of 12 indented bars for each of A and B were incrementally stressed using four-point bending until cracks reached the critical state. Normally the specimens were stressed to the predetermined peak stress with the crosshead speed of 0.05 mm min^{-1}, and then were unloaded as soon as the peak stress was reached. After each stress increment, the specimen was removed from the fixture and the crack length was measured using optical microscopy.

The crack-growth resistance parameter, K_R, was calculated as follows. The total stress intensity factor, K_T, for an indentation crack is the sum of the bending stress intensity factor, K_b, and the residual stress intensity factor, K_r [12–14]

$$K_T = K_b + K_r = \sigma Y c^{1/2} + \S_v(E/H)^{1/2}(P/c^{3/2}) \quad (1)$$

where Y is a shape factor of crack geometry and $\S_v$ is a parameter which depends on the response of the material to the indentation, c, σ, E and H are the crack length, the applied stress, Young's modulus and the Vickers hardness, respectively.

A Vickers indentation crack can propagate stably up to ≈2.5 times its initial length, c_o, as long as the following condition is satisfied [12–14]

$$\frac{dK_T}{dc} < \frac{dK_R}{dc} \quad (2)$$

In this stable growth region, a crack stops propagating whenever $K_T < K_R$. Therefore, the R-curve of a material can be obtained by successively increasing the applied stress on a given crack, measuring the crack sizes, and calculating $K_R (= K_T)$ using Equation 1. In this study, the K_R value, based on the first crack opening at each indentation load, was not included when plotting R-curve, because it may be affected by residual stress formed in the specimen. Also, the values of Y and $\S_v$ were assumed to be constant: 1.174 [15] and 0.016 [13], respectively.

3. Results and discussion

3.1. Characterization of microstructure and large elongated grains

The room-temperature properties of silicon nitrides A and B are presented in Table I. All materials were nearly 100% dense. The fracture toughness was measured using single-edge precracked beam (SEPB) [16].

Scanning electron micrographs of polished and plasma-etched surfaces are shown in Fig. 1. As shown, both specimens had an *in situ* composite microstructure consisting of small matrix grains and large elongated grains. However, silicon nitride B had a coarser microstructure.

Image analysis of the large elongated grains was conducted to evaluate the microstructure quantitatively. Image analysis of the small matrix grains was not considered, because the contribution of small matrix grains to the fracture resistance was minor compared to that of the large elongated grains. It was difficult to evaluate statistically the occasional very large grains found in silicon nitride B and these were excluded in the present treatment. The grain-diameter distribution and aspect-ratio distribution for each material were obtained. Grain diameter was evaluated as the thickness observed in a two-dimensional cross-section. The frequency distribution was expressed in terms of the percentage of the total area occupied by grains of the same diameter size. An area per cent expression in a two-dimensional observation approximately corresponds to volume per cent in a three-dimensional observation [17]. Fig. 2 shows the grain-diameter distribution for silicon nitrides A and B. Silicon nitride A had an elongated grain-diameter

TABLE I Mechanical properties of the silicon nitride materials used in this study

Material	Young's modulus (GPa)	Bending strength (MPa)	Fracture toughness[a] (MPa $m^{1/2}$)
A	290	880	7.0
B	290	678	8.0

[a]Measured by SEPB method.

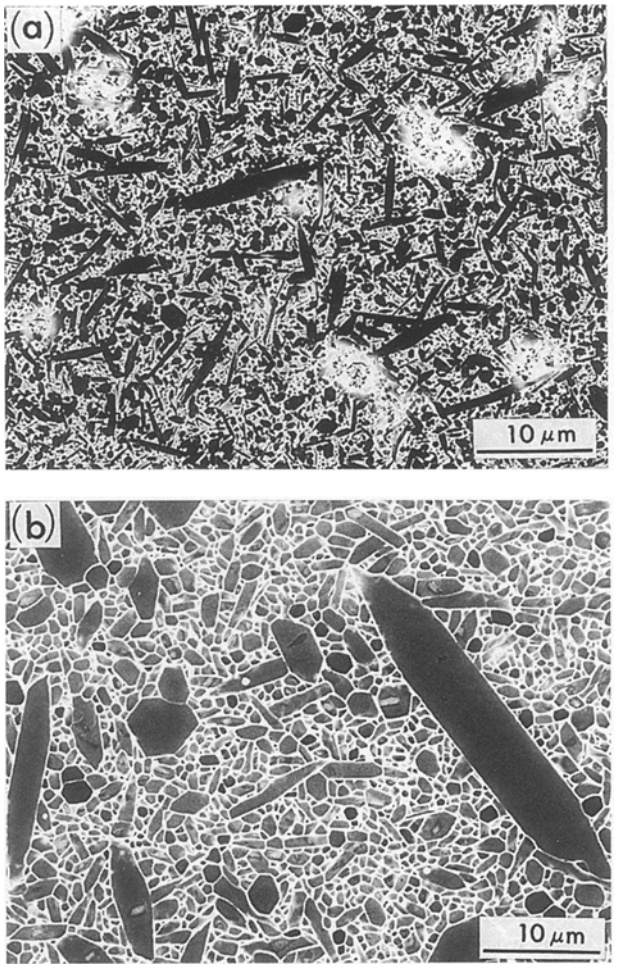

Figure 1 Typical microstructures of polished and etched silicon nitride surfaces: (a) A and (b) B.

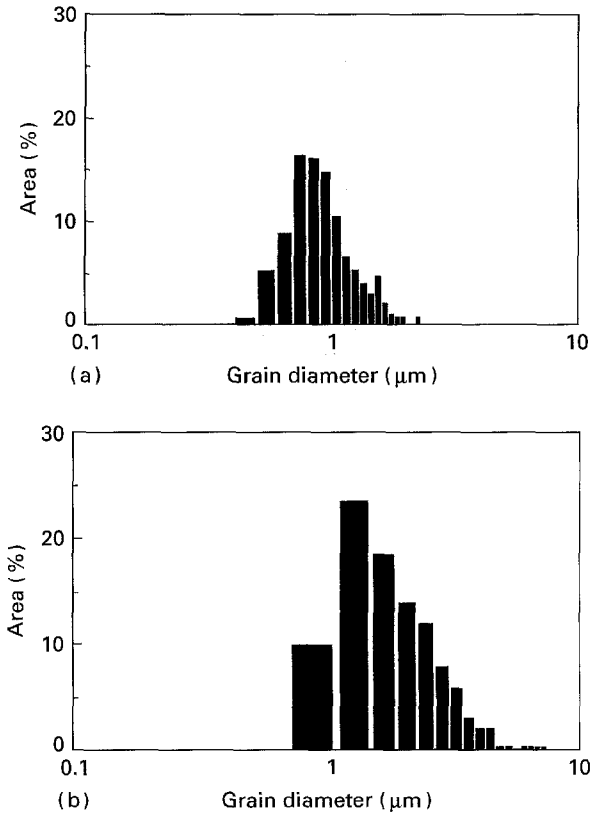

Figure 2 Grain-diameter distribution of large grains in silicon nitrides (a) A and (b) B.

distribution from 0.4–2.2 μm. On the other hand, silicon nitride B had an elongated grain-diameter distribution from 0.8–7.2 μm. The mean aspect ratio of large elongated grains was estimated for both materials. The aspect ratio measured in a two-dimensional cross-section is not equal to the true aspect ratio in three dimensions. In such a case, the mean value of the 10% highest observed ratio (length/diameter) was shown to be the mean of the real aspect ratio [18, 19]. Table II shows the average diameters, the calculated average aspect ratios and average lengths of the large elongated grains for both materials. Silicon nitrides A and B had a similar aspect ratio, but silicon nitride B had a diameter approximately twice that of silicon nitride A.

3.2. Indentation load and strength

The fracture strength versus indentation load for silicon nitrides A and B is shown in Fig. 3. The natural strengths of both materials were arbitrarily plotted at $P = 1$ N. Every specimen was checked to ensure that fracture was initiated from the indent. Bending strength for silicon nitride A reached to its natural strength at 2.94 N indentation. However, bending strength for silicon nitride B reached to its natural strength at 4.9 N indentation. This result suggests that silicon nitride B, which has coarser microstructure, is a more damage tolerant material than silicon nitride A. It is also supported by the crossover of strength, which takes place between 49 and 98 N. Initially silicon nitride A has about 23% higher strength than silicon nitride B. However, after 98 N indentation, silicon nitride A loses about 66% of its initial strength,

TABLE II Average diameter, average aspect ratio and average length of large elongated grains in silicon nitrides A and B

Material	Average diameter (μm)	Average aspect ratio	Average length (μm)
A	0.95 ± 0.31	5.6	5.3
B	2.01 ± 0.98	5.9	11.9

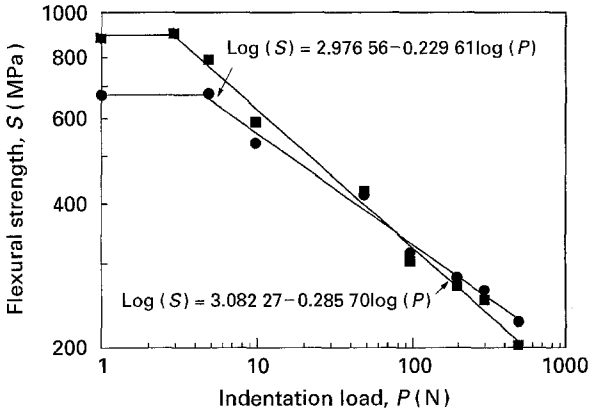

Figure 3 Plots of strength, S, versus indentation load, P, for silicon nitrides (■) A and (●) B. The natural strengths were arbitrarily plotted at $P = 1$ N.

while silicon nitride B loses about 52% of its initial strength and becomes a stronger material than silicon nitride A. Large elongated grains in silicon nitride with a coarser microstructure are believed to act as fracture origins [10]. Fig. 4 shows the typical fracture origin of silicon nitrides A and B. Fracture origins are mostly pores in silicon nitride A and mostly large elongated grains in silicon nitride B as expected. The critical flaw (mostly large elongated grains) size of silicon nitride B is larger than that (mostly pores) of silicon nitride A. Hence, it is reasonable that silicon nitride B is more damage tolerant than silicon nitride A. The above results also suggest that silicon nitride B may have a higher K_R than silicon nitride A.

Linear regression was used to obtain the best fit lines for the data from silicon nitrides A and B. It showed that slopes of silicon nitrides A and B were 0.285 70 and 0.229 61, respectively. Griffith materials, which show no R-curve behaviour, have a slope of 1/3, and R-curve materials have lower slopes [15]. Because the slopes of both materials are less than 1/3, the rising R-curve behaviour is evident for both materials.

3.3. R-curves

Fig. 5 shows fracture resistance measurements as a function of crack length for silicon nitrides A and B.

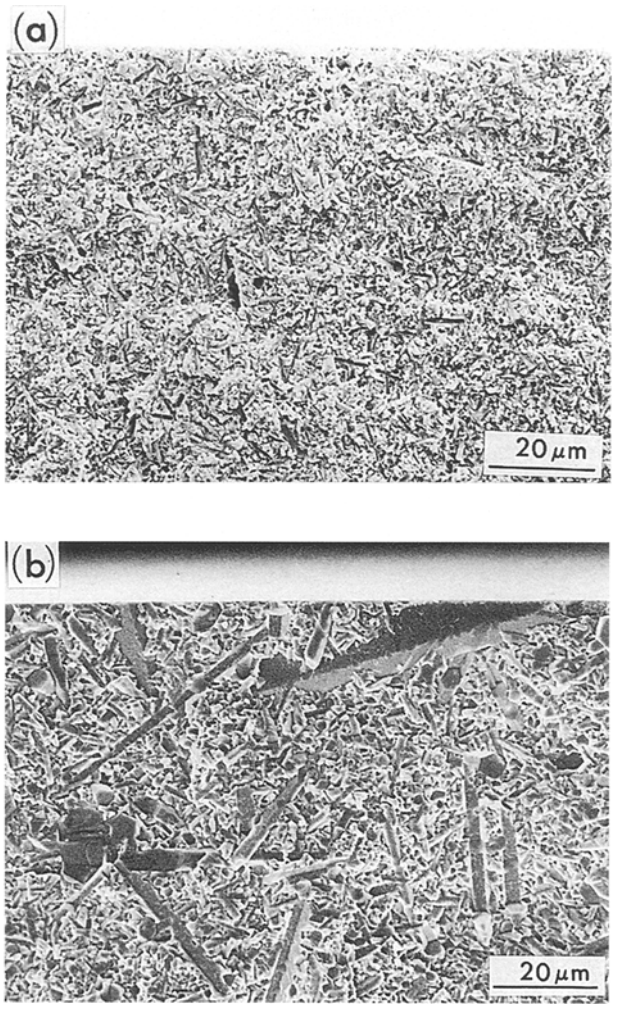

Figure 4 Typical fracture origins of silicon nitrides (a) A and (b) B.

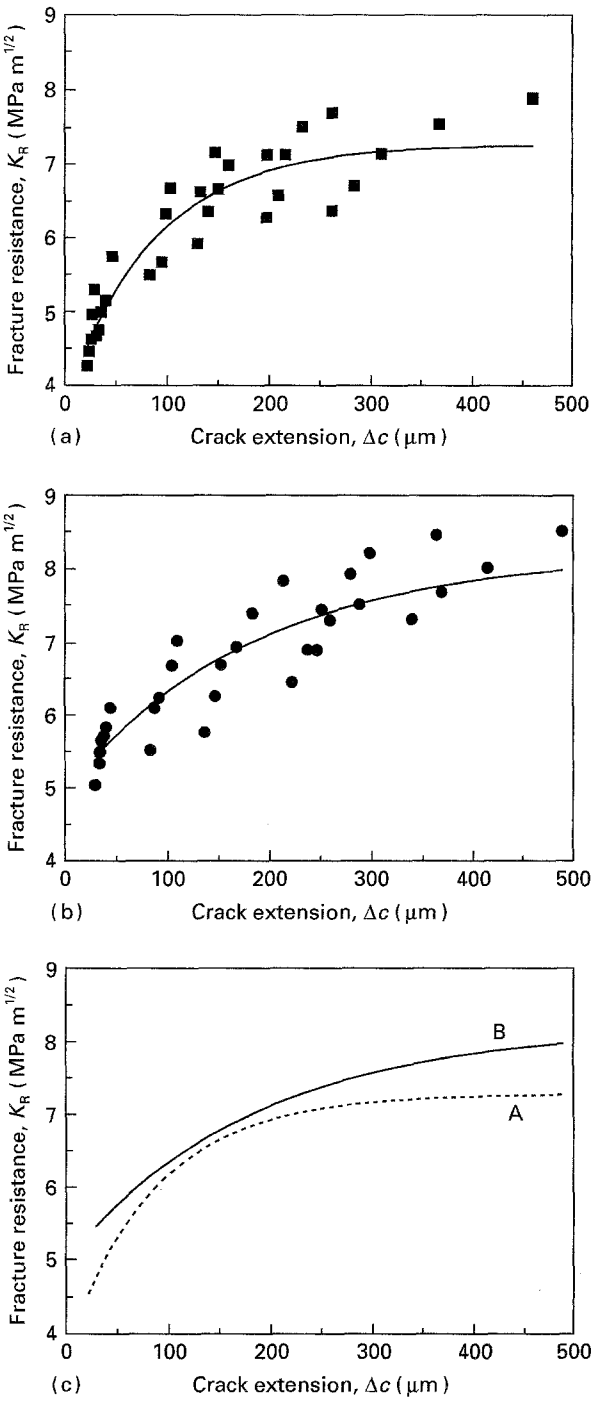

Figure 5 Rising crack-growth resistance curves (R-curve) as a function of crack size for silicon nitrides (a) A and (b) B. (c) Best-fit lines based on the exponential function.

As shown, both materials have the rising crack-growth resistance behaviour, i.e. R-curves. In silicon nitride ceramics with composite microstructure, a principal souce of increased fracture toughness is believed to be grain bridging by elongated grains and/or matrix grains behind the crack tip [1, 20]. As the fracture front advances, the grain bridging sites are left behind and provide a restraining force which must ultimately be overcome for failure to occur. Scanning electron micrographs indicate some evidence of bridging grains in the two silicon nitrides studied here (Fig. 6). We note that at each bridge-rupture site, the cumulative amount of surface-exposed crack length is approximately two to three times the shortest straight-line path through the bridging sites. Moreover, the

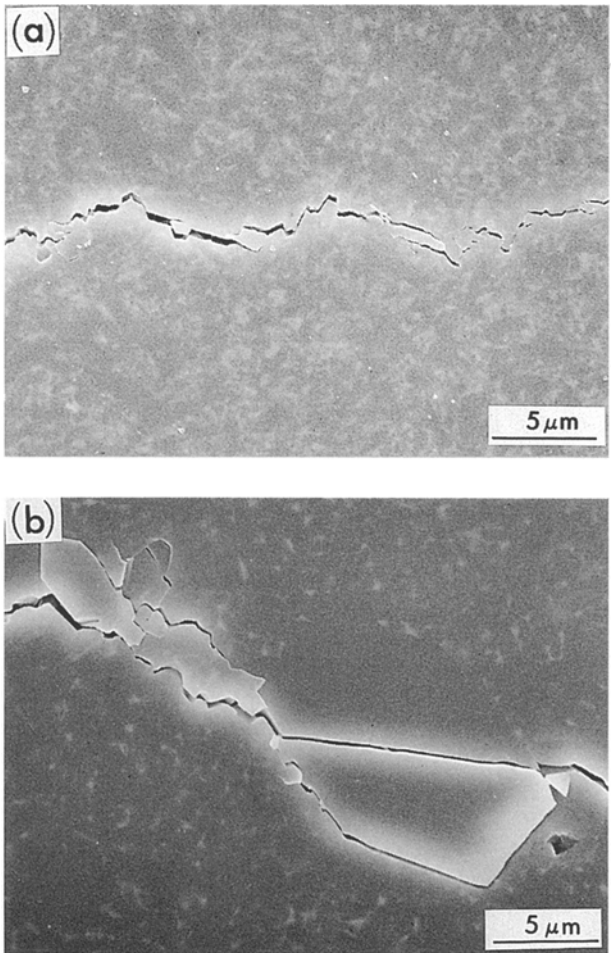

Figure 6 Evidence of grain bridging behind the crack tip for silicon nitrides (a) A and (b) B.

fracture surface area incorporates an amount of transgranular fracture near the bridging grain. Because the grain boundary is weaker than the matrix single crystal (for otherwise most of the fracture would be transgranular), transgranular fracture needs higher energy than intergranular fracture. Therefore, bridges clearly represent an high-energy source of fracture resistance. It is recognized here, of course, that contributions of other toughening mechanisms, for example, crack deflection, cannot be ruled out.

In Fig. 5a and b, the scatter of data is partly a result of the erratic crack-growth behaviour, because the crack extensions depend on the local microstructure. In some cases, the crack would not propagate until a significantly higher stress was applied, indicating strong local crack-growth resistance. No correction of Y and $\S_v$ may also have contributed to the scatter. An estimate of Y was obtained from published stress-intensity factor equations for a surface crack on a specimen subject to a bending moment [21]. Because the variation of the calculated Y values was small ($Y = 1.085$–1.210), Y was set to be constant, $Y = 1.174$ [15], in this study. In general, the indented cracks propagated 1.5–2.7 times the initial crack length before fast fracture. This is in good agreement with the prediction, which is based on the assumption that Y and $\S_v$ are constant [12, 15]. In Fig. 5c, the solid and dotted lines represent the best fit lines of K_R versus Δc data, based on an exponential function suggested by Ramachandran and Shetty [1]. We should point out, however, that the exponential R-curves do not show a correct rising behaviour, when the crack extension is smaller than 50 μm, due to the deficiency of data fitting. The exponential R-curves extrapolate to $K_o \approx 3.78$ and 4.98 MPa $m^{1/2}$ at $c = 0$ for silicon nitrides A and B, respectively. K_o is the intrinsic toughness of the materials.

An interesting feature of the R-curve for both materials was a clear indication of an upper-bound saturation K_R at large crack lengths. The saturated K_R values obtained for silicon nitrides A and B at large crack extension were consistent with the SEPB toughness measured for them. Consider a crack which starts from the indentation crack and which grows with intergranular microfracture to create local bridgings and deflections. The tortuous crack surfaces may be still in physical contact at some locations in the wake and provide a restraining force for crack growth. At first, the growth of the wake zone is correlated with the distance between crack and indentation crack tip, i.e. an increase in macroscopic crack resistance is measured with crack extension. However, crack propagation is accompanied by crack-opening displacement as well as a tortuous crack surface. As a consequence, a maximum interlocking depth of the bridging sites exists beyond which no further interaction occurs. This limits the length of the wake zone and gives rise to the plateau-like saturation behaviour of R-curves [22]. The measured fracture toughness on the low side was, of course, dictated by the lowest indentation load used.

As shown in Fig. 5, silicon nitride B has higher values of K_R than silicon nitride A in the measured crack size range between 30 and 500 μm as expected from the S–P results (Fig. 3).

To determine the microstructural effect on reliability, the relationship between the flexural strength and the crack length after fracture was plotted (Fig. 7). The broken lines in Fig. 7 were plotted using the equation $K_{IC} = 1.35\, S\, c^{1/2}$ for surface flaws of Griffith materials which have no R-curve behaviour and show constant fracture toughness over wide range of crack size [23, 24]. The numbers over the dotted lines are the toughness values. If the processing technique for R-curve materials (silicon nitrides A and B) is equivalent as that for Griffith materials, the strength distribution of the R-curve materials should be narrower, i.e. more reliable, because the slope of the R-curve materials is less steep than that of the Griffith materials in Fig. 7. Also, if the flaw-size distribution in silicon nitrides A and B is equivalent, silicon nitride B should be more reliable than silicon nitride A because the slope of silicon nitride B is less steep than that of silicon nitride A in Fig. 7. Thus coarser microstructure is beneficial to the reliability. However, our results differ from those expected. The strength deviations of silicon nitride A and B were $\pm$ 40.9 and $\pm$ 64.4 MPa, respectively. The Weibull modulus of silicon nitride A was reported to be 23–30 [25], while the Weibull modulus of silicon nitride B was measured as 17. These results are considered to be caused by the wide distribution of

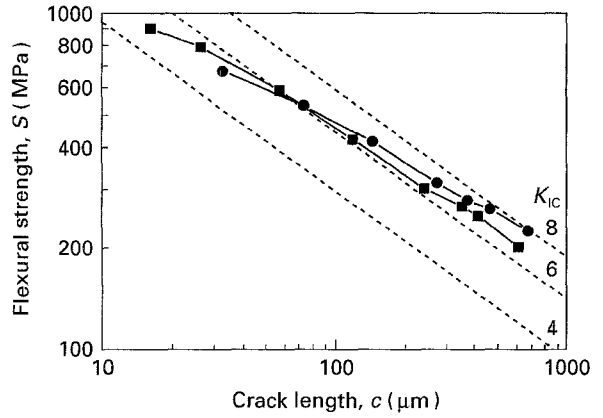

Figure 7 Plots of strength, S, versus crack length, c, for silicon nitrides (■) A and (●) B. Broken lines were plotted using the equation $K_{IC} = 1.35\,S\,c^{1/2}$ for surface flaws of Griffith materials [23, 24].

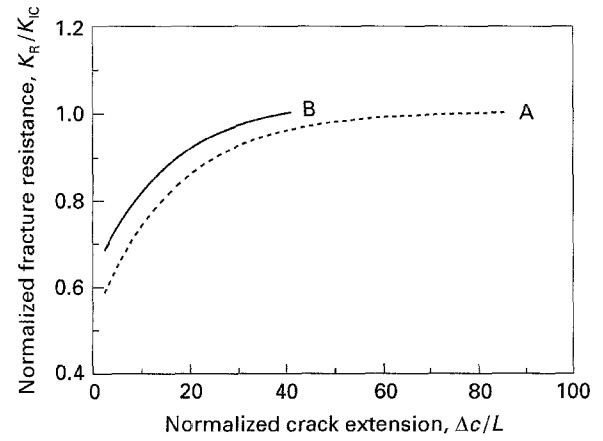

Figure 8 Plots of normalized fracture resistance versus normalized crack extension for silicon nitrides A and B.

critical flaw size in silicon nitride B. When the sintering time is short, the large elongated grains are relatively small in number and size and are dispersed uniformly. However, when the sintering time becomes longer, the large elongated grains grow substantially in size and number and they come into contact and tend to cluster [10]. In silicon nitride B, which was sintered for a relatively long time, i.e. for 8 h at 2000 °C, large elongated grains or a cluster of large grains acted as fracture origins. The average critical flaw size observed in Figs 4 and 7 was 30 μm and about three times larger than the average length of elongated grains, whereas closed pores in silicon nitride A were uniformly dispersed. Hence, it is reasonable for silicon nitride B to have a wide distribution of critical flaw size. The slope of the R-curve around the crack size of a natural flaw is related to the Weibull modulus. Significant increases in the Weibull modulus were observed as the slope of the R-curve increased [6]. However, the above results show that critical flaw-size distribution, as well as the slope of the R-curve, affect the reliability of the materials. These results suggest that the damage tolerance is related to the absolute K_R; however, Weibull modulus is not related to the absolute K_R but to the critical flaw-size distribution as well as the slope of the R-curve at around the critical flaw size. The fracture resistance and crack length in Fig. 5c were normalized by fracture toughness, K_{IC}, and average grain length, L, respectively. The results are shown in Fig. 8, in which large and elongated grains in silicon nitride B are seen to have a larger influence on the fracture resistance. The critical flaws are mostly elongated grains in silicon nitride B and pores in silicon nitride A. It has been shown that the size and distribution of elongated grains are easily controlled by adding nuclei [26]. The optimization of microstructure could be performed in accordance with grain-growth theory.

4. Conclusions

R-curves for two *in situ* reinforced silicon nitrides A and B of different microstructures were characterized using indentation–crack growth measurements. The obtained R-curves showed a higher resistance to crack growth and more damage tolerance for coarser grained silicon nitride B which has 8 MPa $m^{1/2}$ SEPB toughness, compared to that of the finer grained silicon nitride A which has 7 MPa $m^{1/2}$ SEPB toughness. However, silicon nitride A showed a higher Weibull modulus than that of silicon nitride B, due to the relatively narrow critical flaw-size distribution. These results suggest that a coarse microstructure with narrow grain-size distribution is benificial to the toughening, damage tolerance, and reliability. These results also suggest that the damage tolerance is related to the absolute K_R; however, reliability is not related to the absolute K_R but related to the critical flaw-size distribution, as well as the slope of the R-curve, at around the critical flaw size. The damage-tolerant and reliable silicon nitride material may be obtained by tailoring the microstructure with the appropriate R-curve.

Acknowledgement

The stay of Y. W. Kim at NIRIM was supported by the Japan-Korea Industrial Technology Cooperation Foundation (JKF).

References

1. N. RAMACHANDRAN and D. K. SHETTY, *J. Am. Ceram. Soc.* **74** (1991) 2634.
2. H. E. SALIBA, L. CHUCK and N. L. HECHT, *Ceram. Eng. Sci. Proc.* **12** (1991) 1418.
3. C. W. LI, D. J. LEE and S. C. LUI, *J. Am. Ceram. Soc.* **75** (1992) 1777.
4. P. F. BECHER, C. HSUEH, P. ANGELINI and T. N. TIEGS, *ibid.* **71** (1988) 1050.
5. K. T. FABER and A. G. EVANS, *Acta Metall.* **31** (1983) 565.
6. R. F. COOK and D. R. CLARKE, *ibid.* **36** (1988) 555.
7. D. K. SHETTY and J. S. WANG, *J. Am. Ceram. Soc.* **72** (1989) 1158.
8. S. J. BENNISON and B. R. LAWN, *J. Mater. Sci.* **24** (1989) 3169.
9. M. MITOMO and S. UENOSONO, *J. Am. Ceram. Soc.* **75** (1992) 103.
10. N. HIROSAKI, Y. AKIMUNE and M. MITOMO, *ibid.* **76** (1993) 1892.
11. Y. W. KIM, M. MITOMO and N. HIROSAKI, *J. Mater. Sci.* (1994) in press.

12. D. B. MARSHALL and B. R. LAWN, *ibid.* **14** (1979) 2001.
13. G. R. ANSTIS, P. CHANTIKUL, B. R. LAWN and D. B. MARSHALL, *J. Am. Ceram. Soc.* **64** (1981) 533.
14. P. CHANTIKUL, G. R. ANSTIS, B. R. LAWN and D. B. MARSHALL, *ibid.* **64** (1981) 539.
15. R. F. KRAUSE, *ibid.* **71** (1988) 338.
16. T. NOSE and T. FUJII, *ibid.* **71** (1988) 328.
17. N. HIROSAKI, Y. AKIMUNE and M. MITOMO, *J. Ceram. Soc. Jpn* **101** (1993) 1239.
18. G. WÖTTING, B. KANKA and G. ZIEGLER, in "Non-Oxide Technical and Engineering Ceramics", edited by S. Hampshire (Elsevier, London, 1986) p. 83.
19. M. MITOMO, M. TSUTSUMI, H. TANAKA, S. UENOSONO and F. SAITO, *J. Am. Ceram. Soc.* **73** (1990) 2441.
20. P. L. SWANSON, C. J. FAIRBANKS, B. R. LAWN, Y.-W. MAI and B. J. HOCKEY, *ibid.* **70** (1987) 279.
21. J. C. NEWMAN Jr and I. S. RAJU, *Eng. Fract. Mech.* **15** (1981) 185.
22. R. W. STEINBRECH, in "Fracture Mechanics of Ceramics", Vol 9, edited by R. C. Bradt, D. P. H. Hasselman, D. Munz, M. Sakai and V. Y. Shevchenko (Plenum Press, New York, 1992) p. 187.
23. A. S. KOBAYASHI, in "Proceedings of the Second International Conference on the Mechanical Behaviour of Materials" (American Society for Metals, Metals Park, OH, 1976) p. 1073.
24. C. A. ANDERSSON and R. J. BRATTON, in "Science of Ceramic Machining and Surface Finishing II", edited by B. J. Hockey and R. W. Rice (NBS, Gaithersburg, MD, 1979), p. 562.
25. REFERCERAM SN, Japan Fine Ceramic Centre, Nagoya, Japan (1993).
26. N. HIROSAKI, Y. AKIMUNE and M. MITOMO, *J. Am. Ceram. Soc.* **77** (1994) 1093.

Received 21 September 1994
and accepted 28 April 1995